Effect of orographic gravity wave drag on Northern Hemisphere climate in transient simulations of the last deglaciation

Brooke Snoll[1] · Ruza F. Ivanovic[1] · Paul J. Valdes[2] · Amanda C. Maycock[1] · Lauren J. Gregoire[1]

Abstract

Long transient simulations of the last deglaciation are increasingly being performed to identify the drivers of multiple rapid Earth system changes that occurred in this period. Such simulations frequently prescribe temporal variations in ice sheet properties, which can play an important role in controlling atmospheric and surface climate. To preserve a model's standard performance in simulating climate, it is common to apply time dependent orographic variations, including parameterised sub-grid scale orographic variances, as anomalies from the pre-industrial state. This study investigates the causes of two abrupt climate change events in the Northern Hemisphere extratropics occurring between 16 and 14 thousand years ago in transient simulations of the last deglaciation from the Hadley Centre coupled general circulation model (HadCM3). One event is characterized by regional Northern Hemisphere changes comprising a centennial scale cooling of ~ 10 °C across Fennoscandia followed by rapid warming in less than 50 years as well as synchronous shifts in the Northern Annular Mode. The second event has comparable but temporally reversed characteristics. Sensitivity experiments reveal the climate anomalies are exclusively caused by artificially large values of orographic gravity wave drag, resulting from the combined use of the orographic anomaly method along with a unique inclusion of transient orography that linearly interpolates between timesteps in the ice sheet reconstruction. Palaeoclimate modelling groups should therefore carefully check the effects of their sub-grid scale orographic terms in transient palaeoclimate simulations with prescribed topographic evolution.

Keywords Transient simulations of the paleoclimate · Abrupt climate change · Orographic parameterisation · Transient orography · Orographic gravity wave drag · Atmospheric circulation

1 Introduction

Long transient simulations of palaeoclimate are increasingly being performed to better understand the drivers of the sequence of climate events that occurred during the last transition from cold glacial to warm interglacial conditions (e.g. Liu et al. 2009; Menviel et al. 2011; Roche et al. 2011; Bethke et al. 2012; Gregoire et al. 2012; Obase and Abe-Ouchi 2019). Known as the *last deglaciation*, this transition was initiated by a gradual increase in boreal summer insolation ~ 23 thousand years before present (ka BP; Berger 1978), causing the vast ice sheets spanning much of

the Northern Hemisphere continents (Dyke et al. 2002; Lambeck et al. 2014; Hughes et al. 2016) to begin melting (Gregoire et al. 2011). The subsequent increase in atmospheric greenhouse gases (e.g. Loulergue et al. 2008; Schilt et al. 2010; Bereiter et al. 2015) then became the dominant driver of much of the remaining deglaciation (Gregoire et al. 2011).

A particularly compelling characteristic of the last deglaciation is a series of rapid earth system changes, including abrupt (decadal to centennial) hemispheric-scale warmings and coolings of more than 5 °C (de Beaulieu and Reille 1992; Severinghaus and Brook 1999; Lea 2003; Buizert et al. 2014), sudden reorganisations of basin-wide ocean circulation (e.g. Roberts et al. 2010; Ng et al. 2018), and jumps in sea level of tens of metres (e.g. Deschamps et al. 2012; Lambeck et al. 2014). As such, the last deglaciation presents a particularly useful case study for examining and testing our models' abilities to simulate the ice-ocean–atmosphere interactions that operate under warming climates with melting ice sheets and abrupt (human timescale) changes. Yet,

✉ Brooke Snoll
  ee19b2s@leeds.ac.uk

[1] School of Earth and Environment, University of Leeds, Leeds, UK

[2] School of Geographical Sciences, University of Bristol, Bristol, UK

despite decades of research into this most recent period of Earth's geological past, the precise chain of events that followed and their underlying causal mechanisms remain enigmatic (e.g. see discussions in Bethke et al. 2012; Ivanovic et al. 2018; Obase and Abe-Ouchi 2019). Thus, under the auspices of the Palaeoclimate Modelling Intercomparison Project Phase 4 (PMIP4), a protocol was published providing information on how to run transient simulations of the last deglaciation (Ivanovic et al. 2016) to facilitate a coordinated effort for cross-model comparison tapping into the full range of available climate and earth system models as a resource for examining uncertainties in deglacial forcings, trigger mechanisms, and dynamic feedbacks.

One notably complex aspect of simulations of the last deglaciation is the common requirement to prescribe the global distribution of continental ice sheets, including time-evolving orography, as ice mass loading changes. Changes in ice sheet elevation are already considered to be the most important factor to influence atmospheric circulation and sea level pressure (Pausata et al. 2009, 2011; Löfverström and Lora 2017; Gregoire et al. 2018), both potentially deriving from the sub-grid scale parameterisations of anisotropic variations in orographic height (known as orographic variance) within model simulations. For example, Gong et al. (2015) and Gregoire et al. (2018) show through model simulations that higher elevations of the Laurentide and Greenland ice sheets correspond to strong surface wind stress curl over the North Atlantic. Some more recent earth system models demonstrate similar behaviour with the inclusion of dynamic ice sheet models (e.g. see Lofverstrom and Liakka 2018; Lofverstrom et al. 2020; Ackermann et al. 2020; Gregory et al. 2020), and some groups have developed dynamic-continent components within this framework (Meccia and Mikolajewicz 2018). However, ice sheets and their associated geographical features are still mostly externally prescribed in palaeoclimate simulations. If a prescribed ice sheet is required, the PMIP4 protocol for simulating the last deglaciation provides a choice of two global ice sheet reconstructions spanning from 26 ka BP to present, ICE-6G_C VM5a (henceforth 'ICE-6G_C'; Argus et al. 2014; Peltier et al. 2015) and GLAC-1D (Tarasov and Richard Peltier 2002; Tarasov et al. 2012; Briggs et al. 2014; Ivanovic et al. 2016).

As well as orography directly impacting the atmospheric circulation, it can also have an indirect effect via parameterisations of sub-grid scale orographic gravity waves. These waves are generated by flow over orography and transport momentum from their source to where they dissipate or are absorbed, thereby imparting drag on the mean flow (McFarlane 1987). It is necessary to parameterise this momentum transport in atmospheric models due to the spatial scale of the waves being much smaller than the model grid (Kim et al. 2003) and because omitting the drag leads

to climatological biases in circulation (Shaw and Shepherd 2007; Sandu et al. 2016; Pithan et al. 2016), such as excessively strong westerlies in the midlatitude Northern Hemisphere (Kim and Arakawa 1995). Since the first implementation of an orographic gravity wave drag parameterisation in a large-scale model by Boer et al. (1984), multiple other schemes have been developed, for example by Chouinard et al. (1986), Palmer et al. (1986), McFarlane (1987), and Lott and Miller (1997). Most modern general circulation and Earth system models still use variations of these early schemes; for example, the Met Office Unified Model uses a development of the Palmer et al. (1986) scheme but with some improvements to better represent low and mid-level drag (Gregory et al. 1998), and the Lott and Miller (1997) scheme is referenced for the CMIP6 Last Glacial Maximum experiment as described by Kageyama et al. (2017). Orographic variance also impacts form drag, increasing surface friction over rough orographic features. In the Hadley Centre Coupled Model version 3 (HadCM3; Valdes et al. 2017), this is parameterised by increased effective roughness length (Gregory et al. 1998) and depends on the sub-grid scale orographic variance. Despite the abundance of evidence for the importance of orographic gravity wave drag for simulating the general circulation, few studies have examined the interaction between palaeoclimate orographic variations and parameterized orographic gravity wave drag. This stands in sharp contrast to other aspects of palaeoclimate surface and boundary conditions such as ice sheet/shelf extents, coastlines (including inland seas), river routing and bathymetry (e.g. Ivanovic et al. 2016; Kageyama et al. 2017; Menviel et al. 2019).

In this study, we present transient simulations of the last deglaciation using HadCM3 (Valdes et al. 2017), following the PMIP4 protocol (Ivanovic et al. 2016) with the use of ICE-6G_C to define the palaeo ice sheets (Peltier et al. 2015). Unique to these simulations, orography is prescribed as a transient term derived from linear interpolation between the time steps in the reconstruction (every 1000 years 23–21 ka BP and every 500 years thereafter). We show that very small inconsistencies in the calculation of orographic sub-grid scale variances can produce intervals of artificially high orographic gravity wave stress over the North American ice sheet, with profound impacts on the Northern Hemisphere extratropical circulation and regional climates. This phenomenon reaches an extremity at 15.5 ka BP and 14.5 ka BP, with both cases traceable to a spurious behaviour of the orographic gravity wave drag scheme for the prescribed palaeo-orographic boundary conditions.

In the following text, we outline the model set-up and sensitivity experiments used to isolate the cause of this event (Sect. 2), present and discuss our results (Sect. 3), and conclude with a cautionary note that in future simulations with transient palaeogeographies, special care must

be taken in the model set-up of sub-grid scale parameterisations. For brevity, we focus the presented analysis on the 15.5 ka BP event.

2 Methods

2.1 Model description

We performed transient simulations of the last deglaciation with the HadCM3 coupled ocean–atmosphere-vegetation general circulation model (GCM; Gordon et al. 2000; Pope et al. 2000) with modest modifications described by Valdes et al. (2017). This model, often used to simulate palaeoclimates, has an atmospheric resolution of 2.5° latitude by 3.75° longitude with 19 vertical levels starting at the surface and ending at 10 hPa. The ocean's horizontal resolution is 1.25° by 1.25° with 20 vertical layers from the surface of the ocean to ~ 5500 m depth with maximum resolution at the surface. Coupled to the atmospheric GCM, vegetation is represented by the dynamic vegetation model Top-down Representation of Interactive Foliage and Flora Including Dynamics (or TRIFFID) and linked to the land surface with the Met Office Surface Exchange Scheme or MOSES 2.1. Despite its lower resolution, the performance of HadCM3 in simulating mean climate is comparable to other more recent models (Flato et al. 2013; Reichler and Kim 2008), and importantly, it is sufficiently computationally efficient to make it feasible to perform long integrations, such as the 25,000-year long simulations analysed here, within several months.

2.1.1 Orographic gravity wave drag parameterisation in HadCM3

The parameterisation of orographic gravity wave drag in HadCM3 is based upon the scheme implemented in the Met Office Unified Model. The theoretical basis for the gravity wave drag scheme comes from Shutts (1990) and replaces the previous scheme based on Palmer et al. (1986). The four orographic variance terms that relate to the gravity-wave stress are the standard deviation of the sub-grid scale orography (σ), the stress component on the x-plane in the x-direction (σ_{xx}), stress component on the x-plane in the y-direction (σ_{xy}), and the stress component on the y-plane in the y-direction (σ_{yy}). As is customary in palaeoclimate modelling (see discussion in Sect. 1), they are calculated using the data provided by ICE-6G_C as anomalies from pre-industrial, rather than as absolute fields. These four components contribute to the hydrostatic surface stress as given by

$$\tau_{xs} = \frac{\rho_s U_0^3}{\hat{\kappa} \sigma^2 N_s} \hat{h}_1 \hat{h}_2 (\sigma_{xx} \cos\chi + \sigma_{xy} \sin\chi) \tag{1}$$

$$\tau_{ys} = \frac{\rho_s U_0^3}{\hat{\kappa} \sigma^2 N_s} \hat{h}_1 \hat{h}_2 (\sigma_{xy} \cos\chi + \sigma_{yy} \sin\chi) \tag{2}$$

where, ρ_s is the surface values of the density, N_s is the Brunt–Vaisala frequency, U_0 is the component of the wind in the direction of the surface stress, $\hat{\kappa}$ is a typical wavelength for the spectrum of gravity-waves being parameterised, χ is the direction if the surface layer wind relative to westerly, σ is the standard deviation of the sub-grid scale orography, σ_{xx}, σ_{xy}, and σ_{yy} are the squared gradients of the elevation of the sub-grid scale orography.

The values of $\hat{h}_1$ and $\hat{h}_2$ depend on the low-level Froude number and are calculated as:

$$\hat{h}_1 = \frac{N\sigma}{\alpha U_0} \text{ if } < 1 \text{ otherwise, } 1 \tag{3}$$

$$\hat{h}_2 = \frac{N\sigma}{\beta U_0} \text{ if } < 1 \text{ otherwise, } 1 \tag{4}$$

where, α and β are constants to be specified, determining the regime for a given Froude number (Eq. (5), below), N_s is the Brunt–Vaisala frequency, U is the measure of the wind speed of the low-level flow (Walters et al. 2019). The Froude number is defined by

$$F = \frac{U}{(N_s H)} \tag{5}$$

$\hat{\kappa}$ is defined by Shutts (1990) as:

$$\hat{\kappa} = \frac{1}{3} \left[\frac{k_u^{\frac{3}{2}} - k_1^{\frac{3}{2}}}{k_u^{\frac{1}{2}} - k_1^{\frac{1}{2}}} \right] \tag{6}$$

where, k_u is the highest wavenumber lying outside the range of trapped lee waves and k_1 is the lowest unresolved wavenumber of the model.

2.2 Experiment design

2.2.1 Last deglaciation

Simulations of the last deglaciation were run with boundary conditions following the PMIP4 forcing protocol described by Ivanovic et al. (2016). These simulations of the entirety of the last deglaciation began from the end of a previous equilibrium simulation for 23-ka (as described and utilised by Morris et al. 2018) and continued with transient boundary conditions/climate forcings until 2000 years into

the future (3950 CE). For the set of simulations presented here, we use the ICE-6G_C ice sheet reconstruction (Argus et al. 2014; Peltier et al. 2015), which provides the input data for prescribing ice sheet topography and extent, as well as associated boundary conditions (orography, bathymetry, land-sea mask, ocean-mask, and global mean ocean salinity) at 1000 years intervals from 23 to 21 ka BP and 500-year intervals from 21 to 0 ka BP. Orbital parameters (as per Berger 1978) evolve smoothly towards present, and trace gases [with CO_2 as per Bereiter et al. 2015; CH_4 as per Loulergue et al. 2008; and N_2O as per Schilt et al. 2010; all on the AICC2012 timescale of Veres et al. (2013)] transition linearly between published measurements. The solar constant is fixed at the preindustrial value of 1361.0 W/m². Ice sheet meltwater inputs to the ocean follow the 'melt-uniform' scenario proposed by Ivanovic et al. (2016), where we prescribe global mean ocean salinity according to a linear interpolation of the change in ice volume between the ICE-6G_C time-steps. Any difference between this target global mean salinity (from ICE-6G_C) and simulated global mean salinity is redistributed evenly across the entire volume of the ocean at each timestep. There remains significant uncertainty in the history of freshwater forcing from deglaciating ice sheets (e.g., discussion by Ivanovic et al. 2016), and we ran several other meltwater forcing and meteoric river routing scenarios to test its impact on our simulations, including versions of the alternative 'melt-routed' scenario proposed by Ivanovic et al. (2016). In terms of the processes presented in this study, all of these simulations yielded the same results, thus for succinctness and clarity, we present the analysis of just one 'melt-uniform' freshwater-forcing scenario, henceforth referred to as *degl*.

Every time we make an adjustment to the model's boundary conditions (i.e. when implementing changes in land-sea mask, bathymetry, and ocean-mask at the 1 ka intervals 23–21 ka, and 500-year intervals thereafter), we branch off the simulation to produce an overlapping 50-year segment where these boundary conditions are not changed. Thus, by comparing the overlapping 50 years, we can verify the effects of introducing the new paleogeographic configurations, and evaluate the magnitude of any resulting climate-shock (e.g. as discussed/shown in the climate forcing used by Gregoire et al. 2012, 2016).

2.2.2 Orography boundary condition

To incorporate the changes in ice sheet elevation into the climate model, it is common to apply these reconstructions as anomalies from the pre-industrial state. This is advocated for most of the simulations supported by PMIP4. In such cases, the orographic height for a time period is equal to the present-day orography (as in the "control" model simulation) plus the change of height as defined by

the appropriate protocol. Thus, the total elevation at any given time period is the pre-industrial elevation plus the change in elevation given by the reconstruction (suitably regridded onto the model grid). This methodology preserves the model's present-day configuration and hence does not require rerunning the pre-industrial control.

We also must calculate several components of the sub-grid scale orographic variations, and this is more problematic. An ice sheet will typically be relatively smooth in its interior but with large sub-grid scale variability at its edges. Hence in general, we would expect the variances to be smaller than present day in the interior of an ice sheet but large around the edge. It is further complicated in high mountain regions where the mountain peaks may extend beyond the ice sheet itself. The fundamental problem is that high spatial resolution orographic data (typically 10 km or less) is required to calculate sub-grid orographic variances and these are not available for paleo time periods. Some paleo boundary conditions may be presented at sufficiently high resolution (e.g. ICE-6G_C is 10 min resolution and GLAC-1D is 0.5°) but in practice there is often relatively little variance at these fine resolutions. Hence it is not possible to accurately calculate the variances from any existing paleo datasets, and modelling protocols vary in terms of prescriptive. The PMIP4 *LGM* protocol (Kageyama et al. 2017) recommends applying the 10-min orographic differences to an existing present-day orography field, and subsequently smoothing the data using a Gaussian filter, but this will potentially result in an underestimate of total variability. Alternatively, the PMIP4 *last deglaciation* protocol (Ivanovic et al. 2016) specifies using the anomaly method. Since we are performing PMIP4 last deglaciation simulations, we choose to follow this latter approach, and thus determine all variance terms by calculating the change in orographic variance and adding it to the existing pre-industrial values. This will also likely underestimate change because if the anomaly in σ^2, σ_{xx}, or σ_{yy} results in the totals becoming less than zero, they are reset to zero, but it otherwise preserves the total variability.

The total orography elevation and variances (pre-industrial + anomaly) are then applied to the model. The input data is at every 500 years. Rather than having abrupt elevation (and variances) changes every 500 years, every month we linearly time interpolate all orographic fields so that all vary gradually and smoothly between the 500-year tie-points. An example of the evolution of these fields are given in Fig. 5b, which shows the time evolution of in σ^2 and the maximum of σ_{xx}, or σ_{yy} for a specific locality. Note that the variations of the max(σ_{xx}, σ_{yy}) is linear, whereas the σ^2 varies quadratically because the time interpolation is linear in σ.

2.2.3 Sensitivity experiments

In addition to the full-deglaciation simulations described above, we ran multiple shorter sensitivity experiments to isolate the cause of the abrupt climate change simulated at ∼ 15.5 ka (Table 1). These simulations were performed with the atmospheric GCM only to remove the potential influence of the ocean. Therefore, for the ocean boundary conditions, the sensitivity experiments use the equilibrium climate produced by a steady-state simulation of 16 ka (equivalent to the one used by Morris et al. 2018). Our control simulation for these tests, known as '*a-control*', is set with 15.5 ka BP initial boundary conditions and integrated for 100 years. We ran an additional control experiment, known as '*15.45_control*', which was set with the same initial climate conditions as *a-control* and integrated for 100 years, but has 15.45 ka BP boundary conditions imposed. This experiment provides a baseline for assessing the change in the surface climate after the abrupt 15.5 ka BP warming event and further proves that the ocean does not have a major influence on the anomalies. *15.45_control* forms the basis for nineteen additional simulations that systematically vary the atmospheric boundary conditions with respect to the control, homing in on sub-grid scale

Table 1 Details of sensitivity experiments

Simulation	Orographic conditions	RAGS/orbit conditions	TRIFFID conditions	SST/sea ice conditions
a-control	Fixed at 15.5 ka BP	At 15.5 ka BP		
15.45_control	Fixed at 15.45 ka BP	At 15.45 ka BP		
RAGS_constant	Fixed at 15.45 ka BP	At 15.5 ka BP	At 15.45 ka BP	At 15.45 ka BP
TRIFFID constant	Fixed at 15.45 ka BP	At 15.5 ka BP	At 15.5 ka BP	At 15.45 ka BP
SST_ice_constant	Fixed at 15.45 ka BP	At 15.5 ka BP		
orog_var_constant	All variances held at 15.5 ka BP	At 15.5 ka BP		
all_but_US_Asia_orog_constant	All orography at 15.5 ka BP conditions except for Northern Hemisphere between USA and Asia	At 15.5 ka BP		
Fenn_orog_constant	Fennoscandia also held at 15.5 ka BP	At 15.5 ka BP		
UK_Iceland_orog_constant	UK and Iceland also held at 15.5 ka BP	At 15.5 ka BP		
Greenland_org_constant	Greenland also held at 15.5 ka BP	At 15.5 ka BP		
East_NA_orog_constant	Eastern North America also held at 15.5 ka BP	At 15.5 ka BP		
West_NA_orog_constant	Western North America also held at 15.5 ka BP	At 15.5 ka BP		
sd_orog_only	All variances at 15.5 ka BP except the σ at 15.45 ka BP	At 15.5 ka BP		
GWxx_orog_only	All variances at 15.5 ka BP except σ_{xx} at 15.45 ka BP	At 15.5 ka BP		
GWxy_orog_only	All variances at 15.5 ka BP except σ_{xy} at 15.45 ka BP	At 15.5 ka BP		
GWyy_orog_only	All variances at 15.5 ka BP except σ_{yy} at 15.45 ka BP	At 15.5 ka BP		
silhouette_orog_only	All variances at 15.5 ka BP except silhouette at 15.45 ka BP	At 15.5 ka BP		
peak-to-trough_orog_only	All variances at 15.5 ka BP except peak-to-trough at 15.45 ka BP	At 15.5 ka BP		
sd_org_all_areas	All at 15.5 ka BP except σ over all locations at 15.45 ka BP	At 15.5 ka BP		
sd_orog_NA_only	All at 15.5 ka BP except σ over North America at 15.45 ka BP	At 15.5 ka BP		
sd_orog_one_grid_pt_only	All at 15.5 ka BP except σ over one grid point at 62.5° N, 123.75° W at 15.45 ka BP	At 15.5 ka BP		

The longitudinal cut-off point for delineating western and eastern North America (for *East_NA_orog_constant* and *West_NA_orog_constant)* is defined at 105° W. For the four orographic variance terms, σ *is* the standard deviation of the sub-grid scale orography (*sd_orog_only*), σ_{xx} is the stress component on the x-plane in the x-direction (*GWxx_orog_only*) σ_{xy} is the stress component on the x-plane in the y-direction (*GWxy_orog_only*), σ_{yy} is the stress component on the y-plane in the y-direction (*GWyy_orog_only*); see Sect. 2.1.1)

orographic variance (defined in Sect. 2.1.1) in increasing detail. All nineteen of these supplementary sensitivity simulations utilise the same initial conditions as *a-control* and are integrated for 100 years, see Table 1 for details.

2.2.4 Calculation of Northern Annular Mode index

We examine the Northern Annular Mode (NAM) which is the dominant mode of variability in the Northern Hemisphere extratropical circulation (Thompson and Wallace 2001). Changes in the NAM represent fluctuations in the distribution of atmospheric mass between mid- and high-latitudes, with a more positive [negative] NAM index indicating a stronger meridional atmospheric pressure gradient from zonally lower [higher] pressure in north to higher [lower] pressure in the south. Following Li and Wang (2003), we calculate the NAM index as the difference in zonal mean sea level pressure at the model grid boxes closest to 35° N and 65° N. Statistical significance of the sensitivity runs was confirmed by performing two-sided t-tests at the 95% confidence level.

3 Results and discussion

In the *degl* simulation, an unexpected abrupt climate change occurs across the Northern Hemisphere between 16 and 15.45 ka BP that does not correspond directly to changes in solar orbit, atmospheric greenhouse gas concentrations, ice extent, bathymetry/coastlines or freshwater forcing from ice sheet melting. The changes in climate over this period are particularly prominent in the North Atlantic and European region in boreal winter, with surface air temperatures over Fennoscandia and the Nordic Seas regions cooling by ~ 10 °C within around 100 years and then suddenly increasing by a similar magnitude in less than a decade (Fig. 1c). The December–January–February mean surface temperature anomalies over Greenland and the Labrador Sea also show significant changes of ~ 2–3 °C in opposing signs. These changes can be compared to the small (0.25 °C) decrease in global mean surface air temperature in boreal winter between 16 and 15.45 ka BP, indicating the strong locality of the climate patterns.

The surface temperature changes are coincident with significant increases in precipitation (Fig. S1) and marked variations in the NAM index (Fig. 1d). During the period of Fennoscandian cooling, the winter NAM trends towards a more negative state (i.e., weakened meridional pressure gradient), decreasing by around 5 hPa, and then increasing very rapidly over a period of around a decade back to a state equivalent to that around 15.8 ka BP. Similar behaviour of a smaller magnitude is evident in boreal autumn and spring. The change in winter NAM index over this period
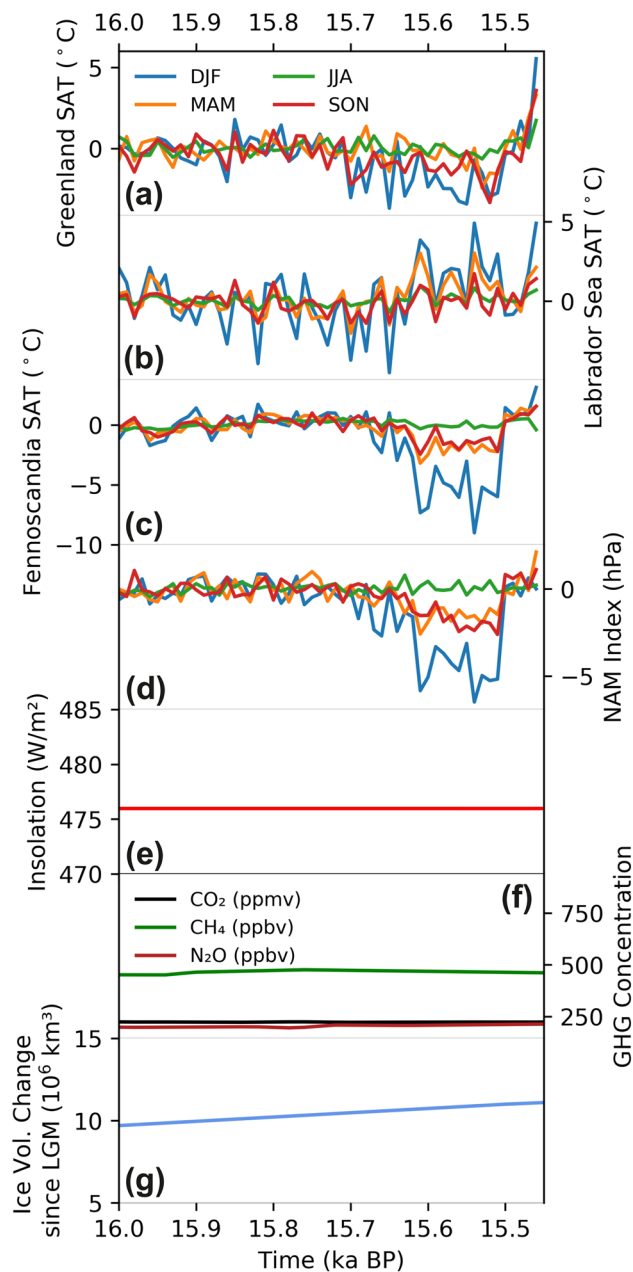

Fig. 1 Model boundary conditions and the resulting abrupt changes in climate. Panels **a**–**c** depict the seasonal decadal mean surface air temperature anomalies relative to the period of stable climate between 16 and 15.8 ka BP in **a** Greenland, **b** the Labrador Sea, and **c** Fennoscandia. Panel **d** as in **a** but for the Northern Annular Mode Index. Panels **e**–**g** depict the boundary condition changes during this time period for **e** June insolation at 60° N (Berger 1978), **f** greenhouse gas concentrations (Loulergue et al. 2008; Schilt et al. 2010; Bereiter et al. 2015; Veres et al. 2013), and **g** ice volume change with respect to the Last Glacial Maximum (LGM, 21 ka BP; Argus et al. 2014; Peltier et al. 2015)

is substantially larger than the magnitude of inter-decadal variability, at ~ 4σ above the decadal average, and is differentiated from the NAM variability over the remainder of

the simulation (though similar variations are seen around 14.5 ka BP when another period of rapid regional climate change is simulated—see Sect. 1).

The spatial patterns of surface climate anomalies during the transition in climate state around 15.5 ka BP are shown in Fig. 2. During the period of Fennoscandian cooling, there is a weakened meridional pressure gradient across the northern extratropics at most longitudes (Fig. 2d). This shows a dominant centre of action in the North Atlantic, resembling the North Atlantic Oscillation (NAO), but interestingly, the dipole in mean sea level pressure (MSLP) also extends across the Eurasian continent, which is not a canonical feature of the NAM (Thompson and Wallace 2001). This

pattern represents a redistribution of atmospheric mass from midlatitudes to high latitudes. During the period of rapid Fennoscandian warming, the pattern of MSLP anomalies is very similar, but opposite in sign (Fig. 2e). Figure 2a and b shows that in the period of a negative NAM trend, there is cooling over western Europe and Fennoscandia, warming over eastern Canada and the USA, and warming over North Africa. This is the canonical pattern of surface temperature anomalies associated with the NAO through modified thermal advection (Thompson and Wallace 2001). Across the Eurasian continent, there is cooling at high latitudes and warming at low latitudes, which reflects reduced poleward heat advection (Fig. 2a). The regional temperature anomalies
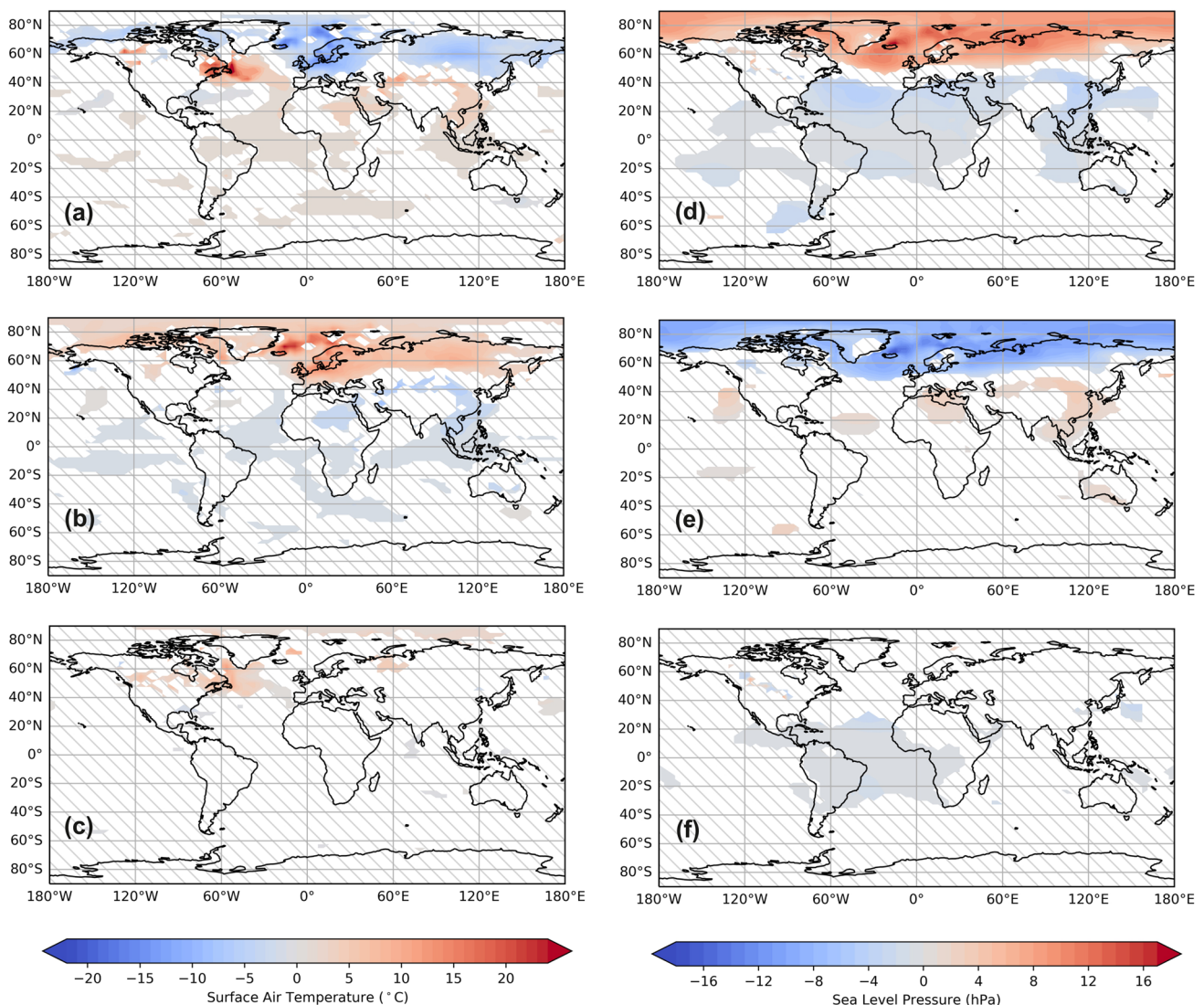
Fig. 2 Change in mean boreal winter (December–January–February) surface air temperature (**a**–**c**) and sea level pressure change (**d**–**f**) for the cooling signal (**a**) and (**d**), the warming signal, (**b**) and (**e**), and the difference between before and after the abrupt event (**c**) and (**f**). The cooling signal depicts the difference between decadal means at 15.8 and 15.5 ka BP. The warming signal depicts the dif-ference between decadal means at 15.5 and 15.45 ka BP, and **c** and **f** depict the difference between decadal means at 15.45 and 15.8 ka BP. Hatching denotes regions where the anomalies are not statistically significant different from a-control at the 95% confidence level using a Student t-test

are reversed in sign in the later period with a rapid increase in NAM (Fig. 2b; although the temperature anomaly over the Western Atlantic is not statistically significant within the natural variability, and therefore is not shown). Hence, the regional surface temperature anomalies appear to be a consequence of the anomalous atmospheric circulation. This is consistent with the radiative forcing being small in this interval (Fig. 1e), and with the changes in global mean surface temperature being small.

The timing of the abrupt changes in climate (Figs. 1, 2) provides a strong indication that this event is not directly driven by ice sheet volume change since there are no coincident large changes in terrestrial ice volume (furthermore, note that there is no surface freshwater forcing from ice sheet meltwater in the PMIP4 'melt-uniform' scenario employed here). Contrary to many of the previous mechanisms identified for driving abrupt transitions in climate in deglacial/glacial simulations, where much larger changes occur, (e.g. Knutti et al. 2004; Liu et al. 2009; Li et al. 2010; Dokken et al. 2013; Obase and Abe-Ouchi 2019), the differences in sea ice concentration, extent and thickness, and the Atlantic meridional overturning circulation over the period of interest (as demonstrated in Fig. S2) are negligible in comparison to the magnitude of the climate change, suggesting that the underlying processes affecting the atmospheric circulation do not originate in the ocean. This is confirmed by the atmosphere-only sensitivity simulations spanning 15.5 ka and 15.45 ka (see Table 1 and Sect. 2.2.3; *a-control* and *15.45_control*), which produce the same anomalies in surface climate despite the absence of a coupled ocean. We next seek to explain the source of the anomalous northern extratropical circulation in the *degl* simulation.

To isolate the causal mechanism, we performed and analysed the 19 additional sensitivity simulations described in Table 1, which hold certain boundary conditions fixed at

15.5 ka BP values, while incrementally updating others to match conditions at 15.45 ka BP. Results from these sensitivity experiments were compared to *a-control,* which uses the full suite of 15.5 ka BP boundary conditions.

The sensitivity experiments that test the effect of radiatively active gases and orbit (*RAGS_constant*), land surface properties (*TRIFFID_constant*), and sea surface temperature and sea ice (*SST_ice_constant*) all show the same North Atlantic climate anomalies as in *degl* (as demonstrated by Figs. 2, 3a). Since orography is the only component not reverted to 15.5 ka BP conditions in these simulations, we determine that the definition of orography must be driving the climate anomalies in this period.

Further sensitivity experiments were performed, iterating from *SST_ice_constant* (where only orography is updated to 15.45 ka BP), to determine which component(s) of the orography fields drive the event. Individual orographic definitions and locations were reverted to 15.5 ka BP conditions, as in *a-control*, in simulations *orog_var_constant*, *all_but_US_Asia_orog_constant*, *Fenn_orog_constant*, *UK_Iceland_orog_constant*, *Greenland_orog_constant*, *East_NA_orog_constant*, and *West_NA_orog_constant*. Although small differences occurred from the changes in orography in each of the experiments, the main features of the abrupt climate event (e.g. Fig. 2b) were present in all simulations except for *orog_var_constant* (Fig. 3b), when all orographic variances are held at 15.5 ka conditions; this demonstrates that the orographic variances are driving the simulated changes of main interest.

To determine precisely which aspect of the orographic variances is key for driving the anomalous atmospheric circulation, further experiments were performed: *SD_orog_only*, *GWxx_orog_only*, *GWxy_orog_only*, *GWyy_orog_only*, *silhouette_orog_only*, and *peak-to-trough_orog_only* (Table 1; as displayed in Fig. 4). In each simulation, all
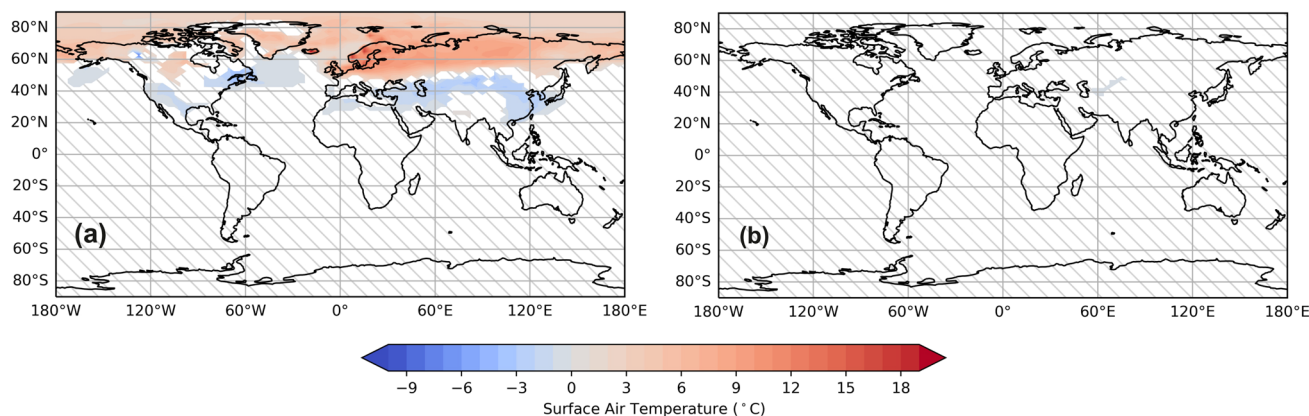

Fig. 3 Change in boreal winter surface air temperature between **a** a-control and SST_ice_constant and **b** a-control and orog_var_constant. Hatching denotes regions where the anomalies are not statistically significantly different from a-control at the 95% confidence level using a Student t-test
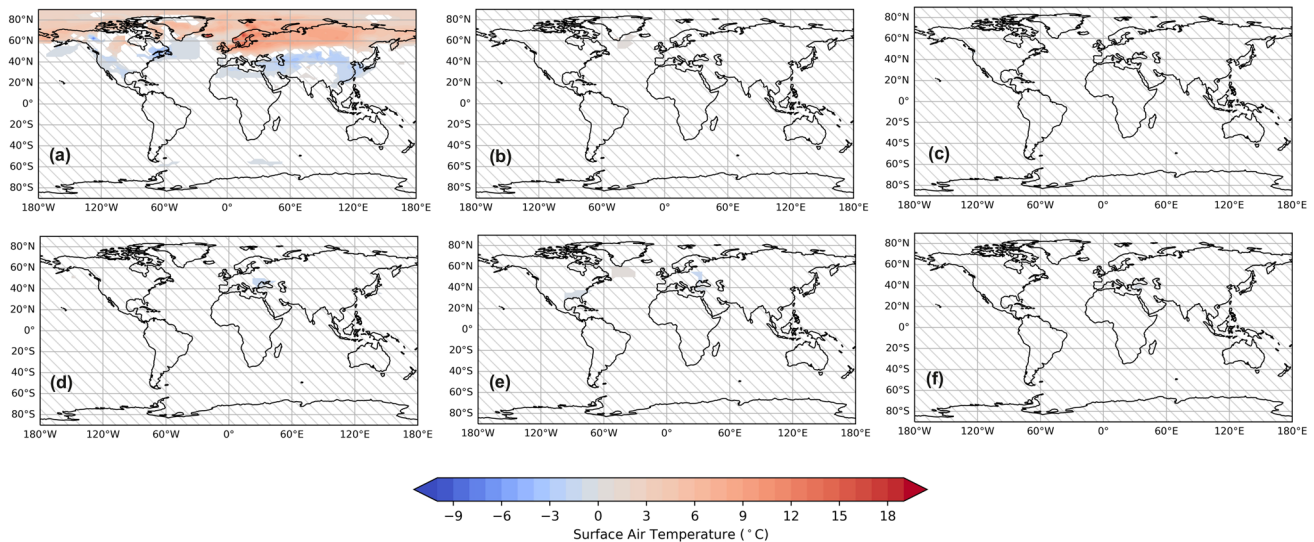
Fig. 4 Impact of individual orographic variances on boreal winter climate, shown as the anomaly of the sensitivity runs with respect to a-control, where the sensitivity run for **a** is sd_orog_only, **b** is GWxx_orog_only, **c** is GWxy_orog_only, **d** is GWyy_orog_only, **e** is silhouette_orog_only, and **f** is peak-to-trough_orog_only. Hatching denotes regions where the the anomalies are not statistically significantly different from a-control at the 95% confidence level using a Student t-test

variances were held at 15.5 ka BP conditions, as in *a-control,* except for the individual parameterisation of orographic variance being tested (σ, σ_{xx}, σ_{xy}, and σ_{yy}, silhouette, and peak-to-trough, respectively), which is set to 15.45 ka BP conditions as in *15.45_control*. As shown in Fig. 4b–f, the adjustments to σ_{xx}, σ_{xy}, and σ_{yy}, silhouette, and peak-to-trough orographic variance all instigate only minor changes in surface temperature that are largely statistically insignificant. Only the standard deviation of the orography (σ) has a strong, and statistically significant, effect on surface air temperature (Fig. 4a), reproducing a similar pattern of climate changes as observed in *degl*.

Based on these results, we conclude that the parameterisation of sub-grid scale orographic variance has a strong influence on climate during the 16–15.45 ka period as simulated in the HadCM3 model. Further simulations *sd_orog_all_areas*, *sd_orog_NA_only*, and *sd_orog_one_grid_pt_only* (Table 1) are used to pinpoint the specific location(s) that influence the climate evolution. Surprisingly, the abrupt climate event as evident in the *degl* simulations and Fig. 2b is closely reproduced in the *sd_orog_one_grid_pt_only* simulation. In this final sensitivity simulation, only the standard deviation of the orography of one grid point in northwestern North America (62.5° N, 123.75° W) is changed to 15.45 ka BP conditions, everywhere else the conditions correspond to those in *a-control* (Fig. 5a). Figure 5b depicts a time series of the orographic variance and hydrostatic stress at the grid box centred over 62.5° N, 123.75° W during the time of the abrupt climate event shown in Figs. 1 and 2. This shows the time evolution of σ^2, the largest of σ_{xx} and σ_{yy} and

the ratio of the two. During the 500-year interval between 16 and 15.5 ka BP, the orographic variance decreases, reaching zero just before 15.5 ka BP. This has a profound impact because the orographic variance provides the denominator of the hydrostatic stress equation (Eqs. 1, 2). Thus, as the orographic variance approaches zero, the hydrostatic stress becomes artificially and unphysically large at a rapidly accelerating rate. This induces a southerly shift in the track of the polar jet stream, which causes the centennial-scale transient reduction in the NAM index and associated cooling over Fennoscandia. When the orographic variance reaches zero at 15.5 ka BP, the orographic gravity wave drag parameterisation is configured to respond by turning off at that location, allowing the westerly winds to quickly resume alongside the recovery of the polar jet stream track, resulting in an instant rebound of the NAM, which drives the abrupt temperature change of ~ 10 °C in Fennoscandia.

Even though the prescription of the orographic variance is not seasonal, there is a pronounced intra-annual asymmetry in the resulting climatic signal, as shown in Fig. 1a–d, with the greatest anomalies occurring in the boreal winter and negligible impact in the June–July–August. In the boreal summer, the low-level westerly winds are located farther south (as illustrated in Fig. S3) causing the U^3 term in Eqs. (1) and (2) to be small, decreasing the overall magnitude of the hydrostatic stress and hence reducing the impact of the temporal evolution in the orographic variance centred at 62.5° N, 123.75° W described above.

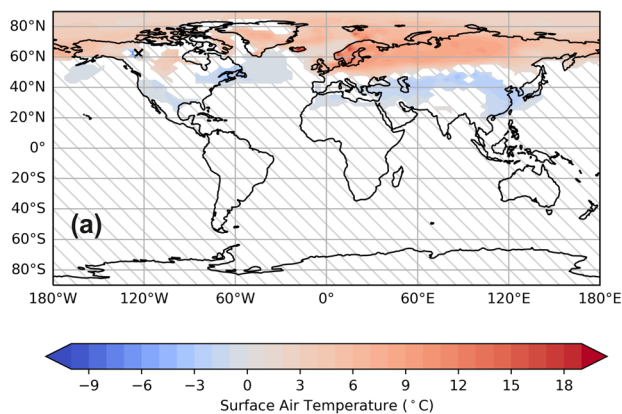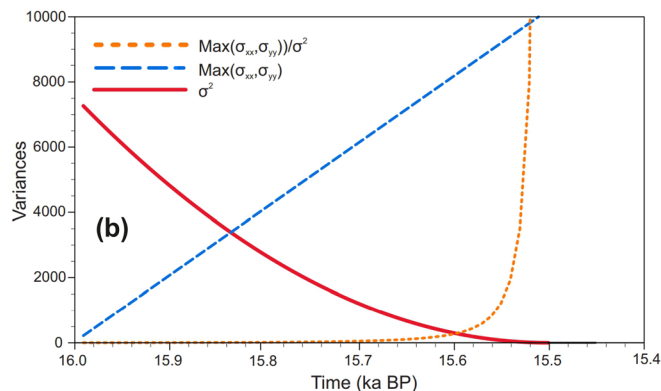The described unphysical growth of the hydrostatic stress is a direct consequence of using the commonly employed

Fig. 5 Results of the sd_orog_one_grid_pt_only sensitivity experiment. **a** Demonstrates the change in surface air temperature between the sensitivity run and a-control. The single grid cell with 15.45 ka BP conditions is indicated by the cross (×; 62.5° N and 123.75° W), conditions everywhere else are kept the same as in a-control. Hatching denotes regions where the anomalies are not statistically significantly different from a-control at the 95% confidence level using a Student t-test. **b** Shows the change in orographic variance in the marked grid cell from 16 to 15.4 ka, where the solid line is the sub-grid scale standard deviation (σ^2), the dashed line is the maximum value of the squared gradients of the elevation of the sub-grid scale orography (max(σ_{xx}, σ_{yy})) and the dotted line is the ratio between the two ((max(σ_{xx}, σ_{yy}))/σ^2). All are at 62.5° N and 123.75° W and the squared gradient (σ_{xx}, σ_{yy}) have been multiplied by 10^5 for plotting

anomaly-from-present method for deriving palaeo-environmental orographic boundary conditions, alongside the application of linear interpolation to smooth fields between time points. The coincidence in location of the unphysical term and the path of the winter low-level westerlies induces the profound effect on atmospheric climate observed in our simulations (with negligible effect on the ocean). We have verified that the similar climate event simulated at 14.5 ka BP in *degl* is also explained by the same technical phenomenon, although from a different change in ice sheet geometry. We do not observe this process at any other time in the 25 ka BP simulation.

The timing of the events at 15.5 ka BP and 14.5 ka BP coincides with key points of deglaciation in the expression of the Laurentide-Cordilleran ice sheet saddle collapse (Gregoire et al. 2012) in ICE-6G_C. Between 16 and 14 ka in the ice sheet reconstruction, ~1500 m of ice is lost in this region. However, at the grid-point of interest (62.5° N, 123.75° W), the ice sheet thins by ~500 m in 500 years between 16 and 15.5 ka BP. Such thinning rates are not unusual in ablation areas over the deglaciation. That such a common change in ice thickness could induce a doubling of the wind stress and such rapid, high amplitude swings in the NAM (producing ~10 °C temperature change over Fennoscandia, ~3 °C over Greenland and ~3 °C over the Labrador Sea, all in a few years, for example) provides a stark but hitherto un-noticed and thus highly useful demonstration of the importance of details in the technical formulation of orographic variance and their relationship to gravity wave drag.

Notably, in the simulations presented here, none of the parameterisations of the sub-grid scale orographic variance terms are out of the ordinary and only smooth transitions between model time steps occur (in part shown by Fig. 5b). Furthermore, the extreme behaviour of the orographic gravity wave drag parameterisation scheme identified at two points in the deglaciation simulation can be hidden at times when other conditions are varying or when extreme climate events are expected/forced to happen (e.g. the Bolling Warming, Meltwater Pulse 1a, Younger Dryas, Dansgaard-Oeschger events more broadly). We determine that the climate transitions seen in our simulations would have been less likely to occur if the orographic fields had been calculated from absolute fields rather than as anomalies from pre-industrial. In addition, because of when they occur in our simulations, we know that they would also not have taken place if orography did not evolve smoothly between each model timestep. These prerequisites, along with the known influence of orographic height on the surrounding atmosphere and surface climate, highlight the importance of carefully checking the evolution and effects of the sub-grid scale orographic terms, especially, for example, when attempting to diagnose the results of a large change in the ice sheets, which may otherwise hide the behaviour found in the *degl* simulations.

4 Conclusions

This study investigated the drivers of two unexpected abrupt climate changes at ~15.5 ka BP and ~14.5 ka BP in a long transient simulation of the last deglaciation performed with the HadCM3 model. The climate anomalies comprise large, rapid changes in the Northern Hemisphere extratropical circulation and associated regional patterns

of surface temperature change. These events are shown to be a consequence of the orographic gravity wave drag parameterisation scheme in the model, resulting from the uniqueness of the prescription of the orographic boundary conditions in these simulations, and the fact that these technical anomalies coincide with the track of the lower level winter westerlies. The combined use of an anomaly method, where sub-grid scale parameterisations are calculated from the data provided in the ice sheet reconstruction as a difference from the pre-industrial, alongside a transient-evolving orography and more frequent than usual time steps in the reconstruction (every 1000 years 23–21 ka BP and every 500 years thereafter) leads to an unrealistic amplification of the hydrostatic stress in the orographic gravity wave drag parameterisation scheme leading to pronounced impacts on the large-scale atmospheric circulation. This study provides an important outlook on the configuration of palaeoclimate simulations and specifically the parameterisation of sub-grid scale orographic variance and its effect on the simulated surface climate. More thorough communication between modellers utilising current models and palaeoclimate modellers using their earlier counterparts could provide more understanding of how parameterisations are implemented, as often the parameterisation set-ups are the same. We have shown that even very small and seemingly physically realistic changes in the orographic variance can cause a surface climate change of ~ 10 °C of local seasonal warming and cooling, a large response to a technical issue that could, in other cases, present itself more modestly. Because the last deglaciation has become a time period of increasing interest due to the series of rapid earth system changes that are scattered throughout, it is crucial to ensure parameterisations are behaving in the manner intended to develop rational and comprehensive hypotheses. As such, these results highlight the importance of checking a model's sub-grid scale orographic variance terms and their effect on the simulated climate when setting up a new geographical configuration in palaeoclimate simulations with prescribed topographic evolution.

Declarations

Conflict of interest The authors have no conflict of interest to declare that are relevant to the content of this article. The authors consent to participation and publication.

Ethical approval Not applicable.

References

Ackermann L, Danek C, Gierz P, Lohmann G (2020) AMOC recovery in a multicentennial scenario using a coupled atmosphere-ocean-ice sheet model. Geophys Res Lett. https://doi.org/10.1029/2019GL086810

Argus DF, Peltier WR, Drummond R, Moore AW (2014) The Antarctica component of postglacial rebound model ICE-6G_C (VM5a) based on GPS positioning, exposure age dating of ice thicknesses, and relative sea level histories. Geophys J Int 198:537–563. https://doi.org/10.1093/gji/ggu140

Bereiter B, Eggleston S, Schmitt J et al (2015) Revision of the EPICA Dome C CO_2 record from 800 to 600 kyr before present. Geophys Res Lett 42:542–549. https://doi.org/10.1002/2014GL061957

Berger A (1978) Long-term variations of daily insolation and quaternary climatic changes. J Atmos Sci 35:2362–2367. https://doi.org/10.1175/1520-0469(1978)035%3c2362:LTVODI%3e2.0.CO;2

Bethke I, Li C, Nisancioglu KH (2012) Can we use ice sheet reconstructions to constrain meltwater for deglacial simulations?:

meltwater in deglacial simulations. Paleoceanography. https://doi.org/10.1029/2011PA002258

Boer GJ, McFarlane NA, Laprise R et al (1984) The Canadian Climate Centre spectral atmospheric general circulation model. Atmos Ocean 22:397–429. https://doi.org/10.1080/07055900.1984.9649208

Briggs RD, Pollard D, Tarasov L (2014) A data-constrained large ensemble analysis of Antarctic evolution since the Eemian. Quat Sci Rev 103:91–115. https://doi.org/10.1016/j.quascirev.2014.09.003

Buizert C, Gkinis V, Severinghaus JP et al (2014) Greenland temperature response to climate forcing during the last deglaciation. Science 345:1177–1180. https://doi.org/10.1126/science.1254961

Chouinard C, Béland M, McFarlane N (1986) A simple gravity wave drag parametrization for use in medium-range weather forecast models. Atmos Ocean 24:91–110. https://doi.org/10.1080/07055900.1986.9649242

de Beaulieu J-L, Reille M (1992) The last climatic cycle at La Grande Pile (Vosges, France) a new pollen profile. Quat Sci Rev 11:431–438. https://doi.org/10.1016/0277-3791(92)90025-4

Deschamps P, Durand N, Bard E et al (2012) Ice-sheet collapse and sea-level rise at the Bølling warming 14,600 years ago. Nature 483:559–564. https://doi.org/10.1038/nature10902

Dokken TM, Nisancioglu KH, Li C et al (2013) Dansgaard-Oeschger cycles: interactions between ocean and sea ice intrinsic to the Nordic seas. Paleoceanography 28:491–502. https://doi.org/10.1002/palo.20042

Dyke AS, Andrews JT, Clark PU et al (2002) The Laurentide and Innuitian ice sheets during the Last Glacial Maximum. Quat Sci Rev 21:9–31. https://doi.org/10.1016/S0277-3791(01)00095-6

Flato G, Marotzke J, Abiodun B et al (2013) Evaluation of Climate Models. In: Intergovernmental Panel on Climate Change (ed) Climate Change 2013 - The Physical Science Basis. Cambridge University Press, Cambridge, pp 741–866

Gong X, Zhang X, Lohmann G et al (2015) Higher Laurentide and Greenland ice sheets strengthen the North Atlantic ocean circulation. Clim Dyn 45:139–150. https://doi.org/10.1007/s00382-015-2502-8

Gordon C, Cooper C, Senior CA et al (2000) The simulation of SST, sea ice extents and ocean heat transports in a version of the Hadley Centre coupled model without flux adjustments. Clim Dyn 16:147–168. https://doi.org/10.1007/s003820050010

Gregoire LJ, Valdes PJ, Payne AJ, Kahana R (2011) Optimal tuning of a GCM using modern and glacial constraints. Clim Dyn 37:705–719. https://doi.org/10.1007/s00382-010-0934-8

Gregoire LJ, Payne AJ, Valdes PJ (2012) Deglacial rapid sea level rises caused by ice-sheet saddle collapses. Nature 487:219–222. https://doi.org/10.1038/nature11257

Gregoire LJ, Otto-Bliesner B, Valdes PJ, Ivanovic R (2016) Abrupt Bølling warming and ice saddle collapse contributions to the Meltwater Pulse 1a rapid sea level rise: North American MWP1a contribution. Geophys Res Lett 43:9130–9137. https://doi.org/10.1002/2016GL070356

Gregoire LJ, Ivanovic RF, Maycock AC et al (2018) Holocene lowering of the Laurentide ice sheet affects North Atlantic gyre circulation and climate. Clim Dyn 51:3797–3813. https://doi.org/10.1007/s00382-018-4111-9

Gregory D, Shutts GJ, Mitchell JR (1998) A new gravity-wave-drag scheme incorporating anisotropic orography and low-level wave breaking: impact upon the climate of the UK Meteorological Office Unified Model. Q J R Meteorol Soc 124:463–493. https://doi.org/10.1002/qj.49712454606

Gregory JM, George SE, Smith RS (2020) Large and irreversible future decline of the Greenland ice sheet. Cryosphere 14:4299–4322. https://doi.org/10.5194/tc-14-4299-2020

Hughes ALC, Gyllencreutz R, Lohne ØS et al (2016) The last Eurasian ice sheets – a chronological database and time-slice reconstruction, DATED-1. Boreas 45:1–45. https://doi.org/10.1111/bor.12142

Ivanovic RF, Gregoire LJ, Kageyama M et al (2016) Transient climate simulations of the deglaciation 21–9 thousand years beforepresent (version 1) – PMIP4 core experiment design and boundary conditions. Geosci Model Dev 9:2563–2587. https://doi.org/10.5194/gmd-9-2563-2016

Ivanovic RF, Gregoire LJ, Burke A et al (2018) Acceleration of northern ice sheet melt induces AMOC slowdown and northern cooling in simulations of the early last deglaciation. Paleoceanogr Paleoclimatology 33:807–824. https://doi.org/10.1029/2017PA003308

Kageyama M, Albani S, Braconnot P et al (2017) The PMIP4 contribution to CMIP6 – part 4: scientific objectives and experimental design of the PMIP4-CMIP6 Last Glacial Maximum experiments and PMIP4 sensitivity experiments. Geosci Model Dev 10:4035–4055. https://doi.org/10.5194/gmd-10-4035-2017

Kim Y-J, Arakawa A (1995) Improvement of orographic gravity wave parameterization using a mesoscale gravity wave model. J Atmos Sci 52:1875–1902. https://doi.org/10.1175/1520-0469(1995)052%3c1875:IOOGWP%3e2.0.CO;2

Kim Y, Eckermann SD, Chun H (2003) An overview of the past, present and future of gravity-wave drag parametrization for numerical climate and weather prediction models. Atmos Ocean 41:65–98. https://doi.org/10.3137/ao.410105

Knutti R, Flückiger J, Stocker TF, Timmermann A (2004) Strong hemispheric coupling of glacial climate through freshwater discharge and ocean circulation. Nature 430:851–856. https://doi.org/10.1038/nature02786

Lambeck K, Rouby H, Purcell A et al (2014) Sea level and global ice volumes from the Last Glacial Maximum to the Holocene. Proc Natl Acad Sci 111:15296–15303. https://doi.org/10.1073/pnas.1411762111

Lea DW (2003) Synchroneity of tropical and high-latitude Atlantic temperatures over the last glacial termination. Science 301:1361–1364. https://doi.org/10.1126/science.1088470

Li J, Wang JXL (2003) A modified zonal index and its physical sense: a zonal index and its physical sense. Geophys Res Lett. https://doi.org/10.1029/2003GL017441

Li C, Battisti DS, Bitz CM (2010) Can North Atlantic sea ice anomalies account for Dansgaard-Oeschger climate signals?*. J Clim 23:5457–5475. https://doi.org/10.1175/2010JCLI3409.1

Liu Z, Otto-Bliesner BL, He F et al (2009) Transient simulation of last deglaciation with a new mechanism for Bølling-Allerød warming. Science 325:6

Lofverstrom M, Liakka J (2018) The influence of atmospheric grid resolution in a climate model-forced ice sheet simulation. Cryosphere 12:1499–1510. https://doi.org/10.5194/tc-12-1499-2018

Lofverstrom M, Fyke JG, Thayer-Calder K et al (2020) An efficient ice sheet/earth system model spin-up procedure for CESM2-CISM2: description, evaluation, and broader applicability. J Adv Model Earth Syst. https://doi.org/10.1029/2019MS001984

Löfverström M, Lora JM (2017) Abrupt regime shifts in the North Atlantic atmospheric circulation over the last deglaciation. Geophys Res Lett 44:8047–8055. https://doi.org/10.1002/2017GL074274

Lott F, Miller MJ (1997) A new subgrid-scale orographic drag parametrization: its formulation and testing. Q J R Meteorol Soc 123:101–127. https://doi.org/10.1002/qj.49712353704

Loulergue L, Schilt A, Spahni R et al (2008) Orbital and millennial-scale features of atmospheric CH_4 over the past 800,000 years. Nature 453:383–386. https://doi.org/10.1038/nature06950

McFarlane NA (1987) The effect of orographically excited gravity wave drag on the general circulation of the lower stratosphere and

troposphere. J Atmos Sci 44:1775–1800. https://doi.org/10.1175/1520-0469(1987)044%3c1775:TEOOEG%3e2.0.CO;2

Meccia VL, Mikolajewicz U (2018) Interactive ocean bathymetry and coastlines for simulating the last deglaciation with the Max Planck Institute Earth System Model (MPI-ESM-v1.2). Geosci Model Dev 11:4677–4692. https://doi.org/10.5194/gmd-11-4677-2018

Menviel L, Timmermann A, Timm OE, Mouchet A (2011) Deconstructing the Last Glacial termination: the role of millennial and orbital-scale forcings. Quat Sci Rev 30:1155–1172. https://doi.org/10.1016/j.quascirev.2011.02.005

Menviel L, Capron E, Govin A et al (2019) The penultimate deglaciation: protocol for Paleoclimate Modelling Intercomparison Project (PMIP) phase 4 transient numerical simulations between 140 and 127 ka, version 1.0. Geosci Model Dev 12:3649–3685. https://doi.org/10.5194/gmd-12-3649-2019

Morris PJ, Swindles GT, Valdes PJ et al (2018) Global peatland initiation driven by regionally asynchronous warming. Proc Natl Acad Sci USA 115:4851–4856. https://doi.org/10.1073/pnas.1717838115

Ng HC, Robinson LF, McManus JF et al (2018) Coherent deglacial changes in western Atlantic Ocean circulation. Nat Commun 9:2947. https://doi.org/10.1038/s41467-018-05312-3

Obase T, Abe-Ouchi A (2019) Abrupt Bølling-Allerød warming simulated under gradual forcing of the last deglaciation. Geophys Res Lett 46:11397–11405. https://doi.org/10.1029/2019GL084675

Palmer TN, Shutts GJ, Swinbank R (1986) Alleviation of a systematic westerly bias in general circulation and numerical weather prediction models through an orographic gravity wave drag parametrization. Q J R Meteorol Soc 112:1001–1039. https://doi.org/10.1002/qj.49711247406

Pausata FSR, Li C, Wettstein JJ et al (2009) Changes in atmospheric variability in a glacial climate and the impacts on proxy data: a model intercomparison. Clim past 14:489–502

Pausata FSR, Li C, Wettstein JJ et al (2011) The key role of topography in altering North Atlantic atmospheric circulation during the last glacial period. Clim past 7:1089–1101. https://doi.org/10.5194/cp-7-1089-2011

Peltier WR, Argus DF, Drummond R (2015) Space geodesy constrains ice age terminal deglaciation: the global ICE-6G_C (VM5a) model. J Geophys Res Solid Earth 120:450–487. https://doi.org/10.1002/2014JB011176

Pithan F, Shepherd TG, Zappa G, Sandu I (2016) Climate model biases in jet streams, blocking and storm tracks resulting from missing orographic drag: missing drag causes model biases. Geophys Res Lett 43:7231–7240. https://doi.org/10.1002/2016GL069551

Pope VD, Gallani ML, Rowntree PR, Stratton RA (2000) The impact of new physical parametrizations in the Hadley Centre climate model: HadAM3. Clim Dyn 16:123–146. https://doi.org/10.1007/s003820050009

Reichler T, Kim J (2008) How well do coupled models simulate today's climate? Bull Am Meteorol Soc 89:303–312. https://doi.org/10.1175/BAMS-89-3-303

Roberts NL, Piotrowski AM, McManus JF, Keigwin LD (2010) Synchronous deglacial overturning and water mass source changes. Science 327:75–78. https://doi.org/10.1126/science.1178068

Roche DM, Renssen H, Paillard D (2011) Deciphering the spatio-temporal complexity of climate change of the last deglaciation: a model analysis. Clim past 6:2593–2623. https://doi.org/10.5194/cpd-6-2593-2010

Sandu I, Bechtold P, Beljaars A et al (2016) Impacts of parameterized orographic drag on the Northern Hemisphere winter circulation. J Adv Model Earth Syst 8:196–211. https://doi.org/10.1002/2015MS000564

Schilt A, Baumgartner M, Schwander J et al (2010) Atmospheric nitrous oxide during the last 140,000 years. Earth Planet Sci Lett 300:33–43. https://doi.org/10.1016/j.epsl.2010.09.027

Severinghaus JP, Brook EJ (1999) Abrupt climate change at the end of the last glacial period inferred from trapped air in polar ice. Science 286:930–934. https://doi.org/10.1126/science.286.5441.930

Shaw TA, Shepherd TG (2007) Angular momentum conservation and gravity wave drag parameterization: implications for climate models. J Atmos Sci 64:190–203. https://doi.org/10.1175/JAS3823.1

Shutts GJ (1990) A new gravity-wave drag parameterization scheme for the Unified Model. TD 204:36

Tarasov L, Richard Peltier W (2002) Greenland glacial history and local geodynamic consequences. Geophys J Int 150:198–229. https://doi.org/10.1046/j.1365-246X.2002.01702.x

Tarasov L, Dyke AS, Neal RM, Peltier WR (2012) A data-calibrated distribution of deglacial chronologies for the North American ice complex from glaciological modeling. Earth Planet Sci Lett 315–316:30–40. https://doi.org/10.1016/j.epsl.2011.09.010

Thompson DWJ, Wallace JM (2001) Regional climate impacts of the northern hemisphere annular mode. Science 293:85–89. https://doi.org/10.1126/science.1058958

Valdes PJ, Armstrong E, Badger MPS et al (2017) The BRIDGE HadCM3 family of climate models: HadCM3@Bristol v1.0. Geosci Model Dev 10:3715–3743. https://doi.org/10.5194/gmd-10-3715-2017

Veres D, Bazin L, Landais A et al (2013) The Antarctic ice core chronology (AICC2012): an optimized multi-parameter and multi-site dating approach for the last 120 thousand years. Clim past 9:1733–1748. https://doi.org/10.5194/cp-9-1733-2013

Walters D, Baran AJ, Boutle I et al (2019) The Met Office Unified Model Global Atmosphere 7.0/7.1 and JULES Global Land 7.0 configurations. Geosci Model Dev 12:1909–1963. https://doi.org/10.5194/gmd-12-1909-2019